Journal of Alloys and Compounds 855 (2021) 157478

Contents lists available at ScienceDirect

Journal of Alloys and Compounds

journal homepage: http://www.elsevier.com/locate/jalcom

Enhancement of thermal stability of Nd–Fe–B sintered magnets with tuned Tb-diffused microstructures via temperature control

Sumin Kim [a, 1], Hyun-Sook Lee [a, 1], Woo Hyun Nam [b], Donghwan Kim [c], Weon Ho Shin [d], Jong Wook Roh [e, **], Wooyoung Lee [a, *]

[a] Department of Materials Science and Engineering, Yonsei University, Seoul, 03722, Republic of Korea
[b] Energy & Environment Division, Korea Institute of Ceramic Engineering & Technology, Gyeongsangnam-do, 52851, Republic of Korea
[c] R&D Center, Star Group, Daegu, 42714, Republic of Korea
[d] Department of Electronic Materials Engineering, Kwangwoon University, Seoul, 01897, Republic of Korea
[e] School of Nano & Materials Science and Engineering, Kyungpook National University, Gyeongsangbuk-do, 37224, Republic of Korea

ARTICLE INFO

Article history:
Received 5 July 2020
Received in revised form
28 September 2020
Accepted 5 October 2020

Keywords:
NdFeB
Grain-boundary diffusion
Thermal stability
Coercivity mechanism
Core–shell microstructure

ABSTRACT

We investigate the magnetic properties and thermal stability of Tb-diffused Nd–Fe–B magnets prepared at various grain-boundary diffusion temperatures and additional heat-treatment temperatures. These heat-treatment processes improved the coercivity of Tb-diffused Nd–Fe–B magnets than that of the base magnets. The diffusion temperature was found to play a key role in controlling the magnetic thermal stability; temperature variations induced precise changes in the decoupled Tb-diffused microstructures in the magnets. The magnet fabricated at a high diffusion temperature showed the best coercivity at room temperature but poor thermal stability. This was due to the formation of Tb-rich (Tb, Nd)$_2$Fe$_{14}$B phases with high magnetocrystalline anisotropy produced inside the grains and less core–shell structures during diffusion at a higher temperature. The best thermal stability was observed for the magnet prepared at a lower diffusion temperature. This magnet had more well-formed core–shell structures than the remaining magnets. By analyzing its microstructure, using electron microscopy and a micromagnetic equation, it was found that a decoupled microstructure with diffused Tb atoms was mainly responsible for the better thermal magnetic stability. Results obtained herein suggest that an optimized diffusion temperature can provide a magnet with good thermal stability.

1. Introduction

The finite availability of fossil fuels and severity of environmental pollution has hastened the development of wind power generation systems and eco-friendly vehicles, such as hybrid or fully electric vehicles [1,2]. Therefore, high-performance Nd–Fe–B rare-earth permanent magnets with high coercivity, which are essential in high-temperature applications such as electric motors and generators, have attracted considerable attention in both academic and industrial fields. To enhance the coercivity of Nd–Fe–B permanent magnets for use at high operating temperatures, high-cost heavy rare-earth elements, such as Dy and Tb, have been added. For this, the grain-boundary diffusion process (GBDP) [3–6] has been studied extensively. As another approach to improve coercivity, the grain refinement method [7–9] has been applied. In particular, GBDP is an effective and simple method for reducing the use of these expensive additives. It enhances coercivity while minimizing the reduction of remanence. The increased coercivity allows the application of Nd–Fe–B permanent magnets in motors for eco-friendly vehicles and actuators. However, in most motor and actuator applications, Nd–Fe–B permanent magnets are often exposed to temperatures above room temperature. Thus, when designing permanent magnets for industrial applications, a range of operating temperatures must be considered because of the temperature dependence of magnetic properties.

Magnetic materials show changes in magnetic properties with an increase or decrease in the temperatures. Permanent magnets lose some proportion of their magnetic performance for every degree of temperature increase. Generally, as the coercivity at room temperature is increased through GBDP and grain refinement, the

* Corresponding author.
** Corresponding author.
E-mail addresses: jw.roh@knu.ac.kr (J.W. Roh), wooyoung@yonsei.ac.kr (W. Lee).
[1] These authors contributed equally.

https://doi.org/10.1016/j.jallcom.2020.157478
0925-8388/

coercivity at higher temperatures is correspondingly increased. However, the increment of room-temperature coercivity does not ensure thermal stability, i.e., retention of coercivity, at higher temperatures. Therefore, coercivity and thermal stability are equally important for magnets in high-temperature applications. Consequently, significant work has been conducted to increase the coercivity and thermal stability of Nd−Fe−B permanent magnets by applying various metal additives [10–13] and low-melting alloys [3–6,14,15]. It is known that the coercivity increment and temperature stability gradually decrease with increasing diffusion depth, due to the influence of microstructures at different depths [15]. Therefore, it is important to analyze the microstructures of magnets along these depths, from the surface, to understand the mechanism of enhanced coercivity and thermal stability.

In this study, we attempted to improve the thermal stability of Nd−Fe−B sintered magnets by simply varying the temperatures of GBDP and additional heat-treatment for Tb diffusion, without any metal and alloy additives. We investigated the magnetic properties and thermal stabilities of Tb-diffused Nd−Fe−B magnets (12 mm × 12 mm × 5 mm) heated at different temperatures, after GBDP had been carried out at various temperatures. The major factor affecting thermal stability was determined by analyzing 1) the microstructure images of the magnets at different depths using electron microscopy and 2) the microstructure-dependent parameters using a micromagnetic equation. Our study confirmed that the decoupled Tb microstructure can be controlled by adjusting the GBDP temperature.

2. Experimental

Before the Tb diffusion process, the surface of a base commercial 48H Nd−Fe−B sintered magnet (12 mm × 12 mm × 5 mm) (Advanced Technology & Materials Co., Ltd.) was carefully etched by ultrasonication for 20 s with a 2% nitric acid solution to improve the coating efficiency of the Tb source materials. A slurry of terbium hydride powder (TbH_2; Lumi M Co., Ltd.) mixed with ethanol (1:1, w/w) was aged for three days to ensure complete extraction of H_2 gas, and this slurry was used as a Tb diffusion source. The sintered magnets were dip-coated in the Tb slurry at 620–940 °C for 6 h in a vacuum of 10^{-6} Torr for GBDP. Then, the sintered magnets were annealed at 820, 920, or 940 °C for 10 h. After the first annealing process, a second heat treatment was performed at 470 °C for 2 h under Ar. The magnets were quenched by a quick injection of cold Ar gas after each heat treatment.

Demagnetization curves were measured by a *B*–*H* hysteresis loop tracer (Permagraph C-300, Magnet-Physik), and temperature-dependent magnetic properties were measured by a magnetic property measurement system (MPMS3-Evercool, Quantum Design Inc.). The irreversible magnetic flux loss was estimated by measuring the flux difference with a Helmholtz coil on the sintered magnets after exposure for 2 h at 180 °C using an electronic flux-meter (EF5, Magnet-Physik). The microstructures of the magnets and distributions of diffused Tb were observed using spherical aberration-corrected scanning transmission electron microscopy (STEM, Titan Themis Z, FEI Corp.) and electron probe microanalysis (EPMA; JXA 8530F, JEOL).

3. Results and discussion

Fig. 1(a) and (b) show the coercivity at room temperature and irreversible flux loss at 180 °C, respectively, for the large-scale Nd−Fe−B sintered magnets (12 mm × 12 mm × 5 mm) prepared at different heat-treatment temperatures of 820, 920, and 940 °C after GBDP in the temperature range of 620–940 °C. As shown in Fig. 1(a), coercivity of all the samples shows an increasing tendency

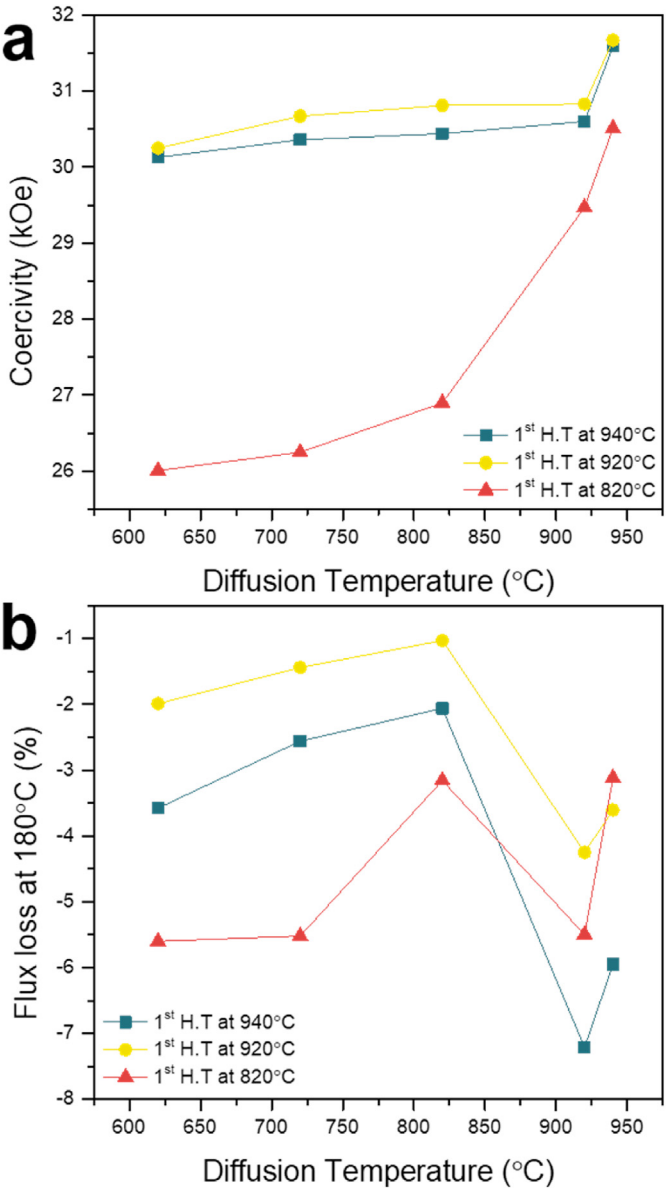

Fig. 1. (a) Coercivity at room temperature and (b) flux loss at 180 °C for the Tb-diffused Nd−Fe−B magnets (12 mm × 12 mm × 5 mm) prepared at different heat-treatment temperatures (820, 920, and 940 °C) after GBDP in the temperature range 620–940 °C.

with an increase in the diffusion temperature of GBDP from 620 to 940 °C. The maximum coercivity, i.e., 31.67 kOe, is observed in the sample heat-treated at 920 °C after GBDP at 940 °C.

When permanent magnets are heated above their maximum operating temperatures but below their Curie temperatures, they experience irreversible losses in magnetic performance. In other words, permanent magnets cooled after heating show decreased performance than that shown before heating. This irreversible loss can theoretically be recovered by remagnetization. However, remagnetization of magnets already positioned in motors or actuators is practically impossible. Therefore, the irreversible flux loss, h_{irr}, is calculated using the following equation [13]:

$$h_{irr} = \frac{\Phi\prime(T_0) - \Phi(T_0)}{\Phi(T_0)} \times 100\% \quad (1)$$

where $\Phi(T_0)$ and $\Phi'(T_0)$ are the flux values at room temperature

before and after exposure to a certain high temperature, respectively. Fig. 1(b) shows h_{irr} for the prepared magnets after 2 h exposure to 180 °C, a harsh environmental condition, with varied diffusion temperatures. As seen in Fig. 1(b), the minimum flux loss (−1.03%) is observed in the sample prepared with the first heat-treatment temperature of 920 °C after GBDP at 820 °C.

Therefore, at the same first heat-treatment temperature of 920 °C, the diffusion temperatures yielding the lowest h_{irr} at 180 °C (820 °C) and highest coercivity (940 °C) differ. This shows that the magnetic properties, which depend on the real operating temperatures of the magnet, are strongly affected by the diffusion temperature. Hereafter, we refer to the magnet with diffusion at 940 °C and heat treatment at 920 °C as the DT940 magnet and the magnet with diffusion at 820 °C and heat treatment at 920 °C as the DT820 magnet.

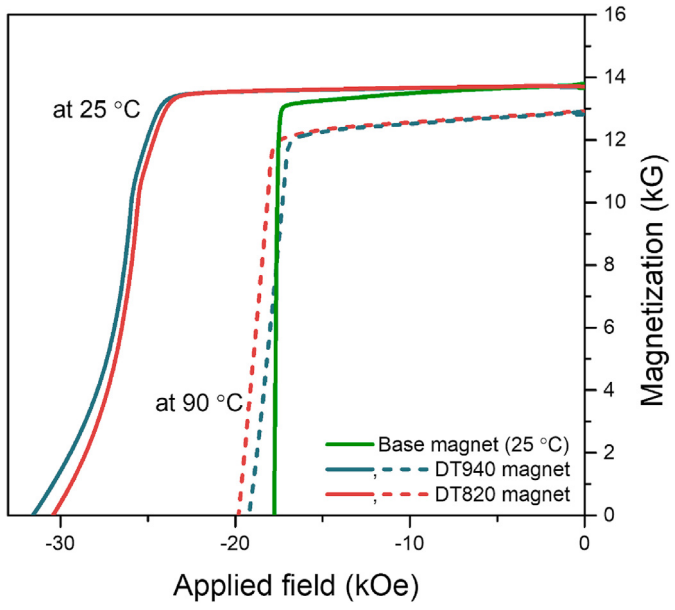

Fig. 2. Demagnetization curves of the base, DT820, and DT940 magnets measured at 25 °C (solid lines) and 90 °C (dotted lines).

Fig. 2 shows the demagnetization curves of the DT820, DT940, and base magnets measured at 25 and 90 °C. From these curves, we obtain the magnetic properties of intrinsic coercivity (H_{cj}), remanence (B_r), and maximum energy product ($(BH)_{max}$) of the prepared magnets, measured at different temperatures of 25 and 90 °C. These values are listed in Table 1. As shown, H_{cj} of the DT820 (30.44 kOe) and DT940 (31.67 kOe) magnets at 25 °C are significantly improved than that of the base magnet (17.92 kOe), whereas B_r and $(BH)_{max}$ are slightly reduced. As the working temperature is increased from 25 to 90 °C, the coercivity of both magnets decrease. In particular, the decrease in H_{cj} of DT940 (19.22 kOe) is larger than that of DT820 (19.81 kOe).

In addition, the magnetic properties of H_{cj}, B_r, and $(BH)_{max}$ are decreased as the temperature is increased from 25 to 90 °C. Therefore, we estimated the loss of thermal stability of the magnets by calculating the temperature coefficients of B_r (α) and H_{cj} (β) according to the following equations [16,17]:

$$\alpha = \frac{B_r(T_2) - B_r(T_1)}{B_r(T_1)(T_2 - T_1)} \times 100(\%) \quad (2)$$

$$\beta = \frac{H_{cj}(T_2) - H_{cj}(T_1)}{H_{cj}(T_1)(T_2 - T_1)} \times 100(\%) \quad (3)$$

The temperature coefficients α and β were estimated for the DT820 and DT940 magnets using the temperature dependence of B_r and H_{cj} measured in the temperature range of 25–180 °C (See Figs. S1 and S2 in Supplementary Material). The α and β coefficients

Table 1
Magnetic properties, flux loss at 180 °C, temperature coefficients of Br (α) and Hcj (β), and squareness factor (SF) for the base, DT820, and Dt 940 magnets.

	DT* (°C)	HT** (°C)	25 °C				90 °C		Flux loss (%)	α (%/°C)	β (%/°C)	Squareness factor (SF)	
			H_{cj} (kOe)	B_r (kG)	$(BH)_{max}$ (MGOe)	H_{cj} (kOe)	B_r (kG)	$(BH)_{max}$ (MGOe)				25 °C	90 °C
Base magnet	-	-	17.92	13.78	46.95	-	-	-	-	-	-	0.98	-
DT 820	820	920	30.44	13.62	46.26	19.81	12.75	39.26	−1.03	−0.098	−0.537	0.81	0.91
DT 940	940	920	31.67	13.65	46.36	19.22	12.74	39.17	−3.61	−0.103	−0.602	0.78	0.88

*DT: Diffusion temperature.
**HT: Heat-treatment temperature.

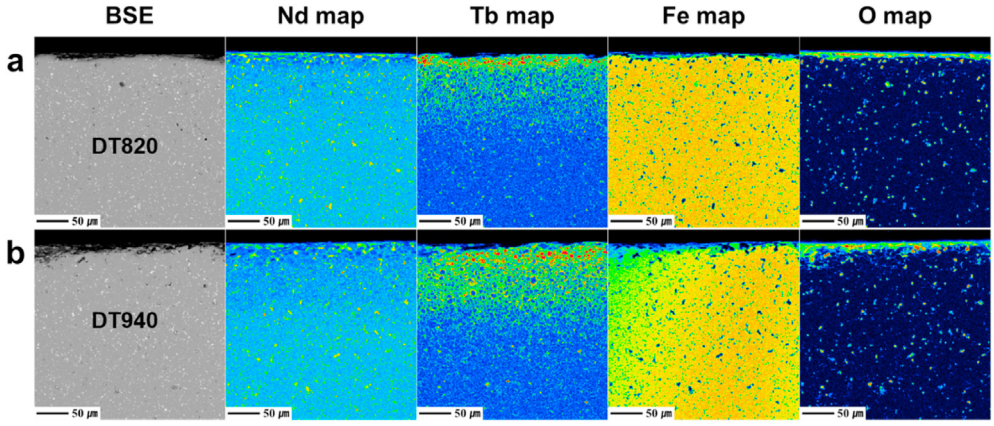

Fig. 3. Cross-sectional EPMA profiles of (a) DT820 and (b) DT940 magnets at depths from 0 to 275 μm.

for the DT820 and DT940 magnets are also listed in Table 1. Both absolute values are higher for the DT940 magnet, which shows the maximum coercivity, than those for the DT820 magnet, which shows the minimum flux loss. This means that the thermal stabilities of B_r and H_{cj} are better for the DT820 magnet than those for the DT940 magnet.

We estimated a squareness factor (SF), which can be quantified by the second quadrant of the hysteresis loop (demagnetization curve) according to the following equation [18–20]:

$$SF = \frac{\mu_0 H_k}{\mu_0 H_{cj}} \quad (4)$$

where $\mu_0 H_k$ is the knee field strength, corresponding to the field at 90% of B_r. SF is associated with tolerances for B_r and H_{cj} values and for the homogeneity of these properties [20]. Thus, the SF values refer to the microstructural homogeneity of the magnet materials [20]. As shown in Table 1, the SF values of the curves in the DT820 magnet (0.81 at 25 °C and 0.91 at 90 °C) are higher than those in the DT940 magnet (0.78 at 25 °C and 0.90 at 90 °C). The SFs of the DT820 and DT940 magnets are increased with increasing temperature. This result indicates that the microstructural homogeneity is improved at higher temperatures. The microstructure of magnets also affects the thermal stability of the magnetic properties. From this viewpoint, microstructural investigation of the magnet along different depths from the surface can help to understand the causes of change in the squareness and magnetic stability in a permanent magnet.

The cross-sectional elemental distributions of the magnets were analyzed using EPMA. Fig. 3 shows the two-dimensional EPMA mapping images of the DT820 and DT940 magnets obtained at the depth of 275 μm from the surface of each magnet. For both the magnets, Nd and Fe show homogeneous distributions. Although both DT820 and DT940 contain O, which seriously promotes the deterioration of magnetic properties, degradation by O is negligible in these samples because of the low concentration and uniform distribution of the element. Significant differences in elemental distribution are observed in the Tb maps. Tb is concentrated within the depth of 100 μm from the surfaces of both magnets, but its detailed distribution differs between the two.

Fig. 4 shows the Tb cross-sectional elemental mapping images and Tb concentration profiles from the surface to the depth of 1300 μm in the DT820 and DT940 magnets. Both the magnets

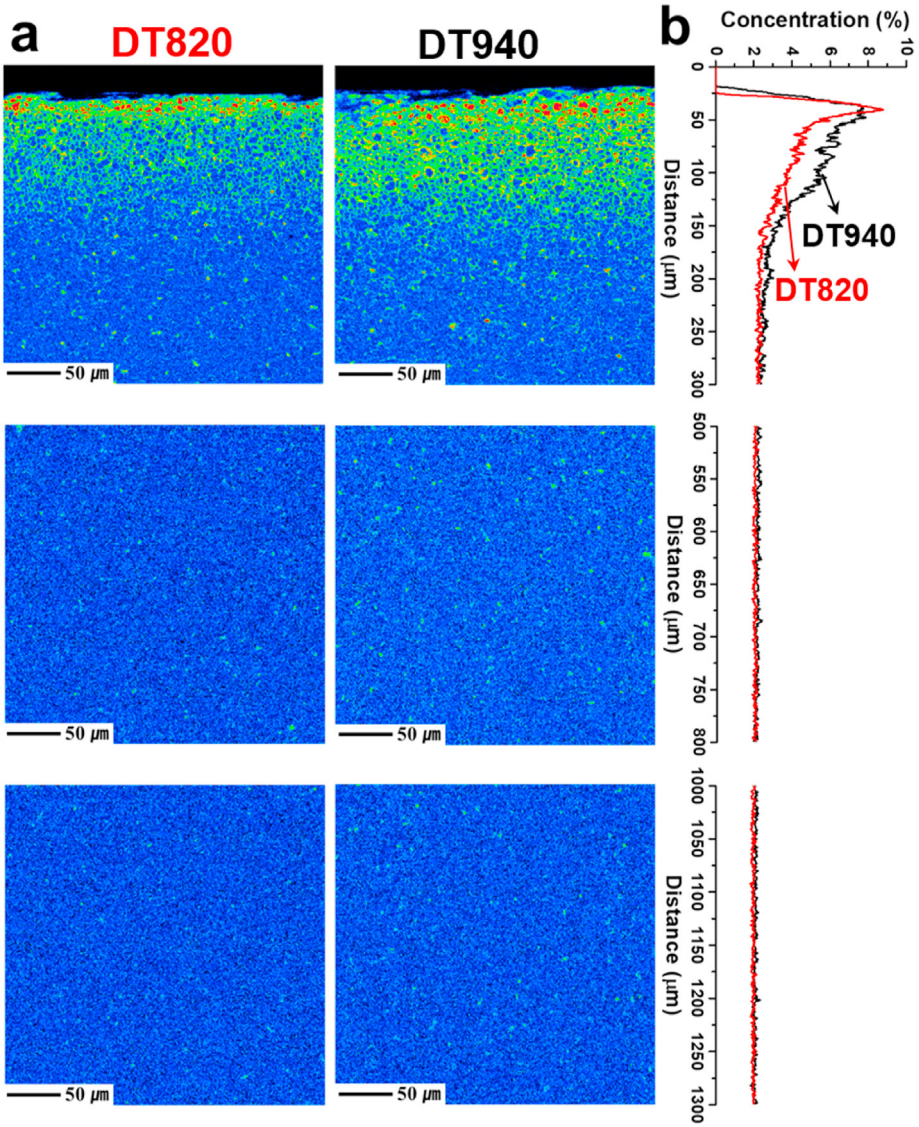

Fig. 4. (a) Tb elemental mapping images and (b) Tb concentration profile along the distance from 0 to 1300 μm from the surface for the DT820 and DT940 magnets.

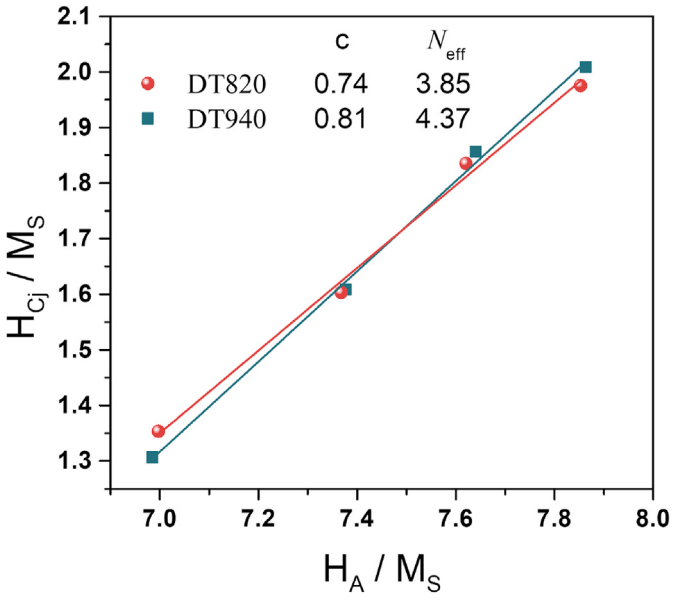

Fig. 5. Dependence of $H_{cj}(T)/M_S(T)$ on $H_A(T)/M_S(T)$ of the as-prepared DT820 and DT940 magnets.

exhibit similar Tb contents and distributions in the depth range of 500−800 μm and 1000−1300 μm. However, a remarkable difference in the elemental distributions of Tb is observed in the 0−300 μm region. Both the magnets have the highest Tb concentrations at depths of ~25 μm from the surface. The concentration of the peak is higher in DT820 (~8.7%) than that in DT940 (~7.6%). At depths beneath the peaks, shoulders continue till the depth of 100 μm. The shoulder of DT820 is lower than that of DT940. The differences in Tb distribution between DT820 and DT940 arise from the different microstructures of the two samples. As shown in Fig. 4, Tb is mainly distributed at the grain boundaries in the DT820 magnet, whereas Tb is located in both the grain boundaries and within grains in DT940. This result indicates that (1) core−shell structures are well formed near the surface of the DT820 magnet by the grain-boundary diffusion of Tb; (2) Tb atoms diffuse into the main phase of $Nd_2Fe_{14}B$ by displacing Nd in the DT940 magnet, generating Tb-rich (Tb, Nd)$_2Fe_{14}B$ grains by Tb through-lattice diffusion under the higher diffusion temperature. Therefore, the higher H_c of DT820 than that of the base magnet at 25 °C could be attributed to the suppressed nucleation of reverse magnetic domains by the core−shell structure. The higher H_c of DT940 than that of the DT820 may be caused by the combined effects of the higher magnetocrystalline anisotropy of (Tb, Nd)$_2Fe_{14}B$ grains and core−shell structure. Additionally, the microstructural distribution of Tb concentrated on the magnet surface can give rise to the tails observed in the demagnetization curves of both magnets at 25 °C, as shown in Fig. 2. In comparison with DT820, DT940 shows a lower SF, which can be attributed to the relatively inhomogeneous distribution of Tb in DT940.

To understand the experimentally observed reverse change in the coercivity of the prepared magnets with increasing temperature, the relationship between coercivity and magnet microstructure was analyzed using a micromagnetic equation based on the nucleation model. The temperature-dependent coercivity can be expressed as follows [3,17,21−23]:

$$H_{cj}(T) = cH_A(T) - N_{eff}M_s(T) \quad (5)$$

where H_A and M_s are the anisotropy field and saturation magnetization, respectively, and c and N_{eff} are microstructure-dependent parameters reflecting the effects of microstructure on coercivity. The parameter c represents the influence of crystallographic defects in the magnetically inhomogeneous region on the grain surface and grain misalignment, whereas N_{eff} describes an effective demagnetization factor related to the stray field at the edges and corners of grains; this stray field assists nucleation of reversed domains. By plotting H_{cj}/M_s vs. H_A/M_s for different temperatures and applying a linear fit to the data, the values of c and N_{eff} are determined for the magnets with different diffusion temperatures (Fig. 5). The obtained values of c and N_{eff} for DT820 and DT940 are given in the inset of Fig. 5.

For DT820, $c = 0.74$, which is lower than that for DT940 ($c = 0.81$), indicating that more crystallographic defects exist at the grain surfaces in DT820. TEM analysis was conducted to investigate the detailed crystallographic structures of the magnets. Fig. 6 shows the results of TEM analysis of DT820. Fig. 6(a) shows a bright-field TEM image of a grain surface comprising Tb-rich (Nd, Tb)$_2Fe_{14}B$ phases, which are generated by replacing Nd with Tb in the main $Nd_2Fe_{14}B$ phase during GBDP and secondary heat treatment. The Tb-rich (Nd, Tb)$_2Fe_{14}B$ phases are inferred from chemical composition analysis via energy-dispersive X-ray spectroscopy line scans (Figs. S3 and S4 in Supplementary Material). Fig. 6(b) and (c) show high-resolution TEM images obtained from the corresponding areas marked *b* and *c* in Fig. 6(a). Fast Fourier transform was applied in the areas indicated by A to F shown in Fig. 6(b) and (c). The corresponding electron diffraction patterns in the selected areas for the [−101] beam direction are shown in the column of Fig. 6(d). The patterns clearly show that the crystals in areas *b* and *c* comprise the tetragonal $Nd_2Fe_{14}B$ phase. However, the orientations of the crystals are slightly rotated relative to each other, as shown in Fig. 6(e). This defect is more prominent in DT820 than that in DT940. This demonstrates that the low *c* value in DT820 can be attributed to the higher density of crystallographic detects at the grain surfaces, as mentioned above.

A larger difference in N_{eff} than that in c is observed in the microstructure-dependent parameters. Therefore, N_{eff} is considered responsible for the main effect on the coercivity in the prepared magnets. The N_{eff} value is mainly governed by factors including grain shape, presence of non-ferromagnetic phases, and intergranular exchange interactions, which affect the dependence of stray fields on neighboring grains [24,25]. Therefore, we performed a more detailed microstructural analysis using submicroscale EPMA at depths of 80 and 300 μm below the magnet surfaces. Fig. 7 reveals a significant difference in the Tb distributions of DT820 and DT940. The sizes and shapes of the grains are similar in both magnets, as shown in the backscattered electron (BSE) images in Fig. 7. The densities and distributions of non-ferromagnetic phases are also similar, as shown in the Nd, Fe, and O maps in Fig. 7. However, in comparison with the DT940 magnet, the DT820 magnet exhibits a higher density of well-formed core−shell structures at depths of both 80 and 300 μm, as shown in the Tb mapping images of Fig. 7. Less lattice diffusion occurs in the DT820 magnet than that in the DT940 magnet, as seen in Figs. 3 and 4. Therefore, the Tb atoms not consumed by lattice diffusion contributed to the formation of the core−shell structures in relatively deep areas within the magnet. The results suggest sufficient isolation between the grains (cores) by the grain boundaries (shells) in DT820. As a result, the exchange decoupling of the magnetic domains of the grains is enhanced in DT820. Therefore, the low N_{eff} value of the DT820 (3.85) than that of the DT940 (4.37) is due to the stronger decoupling effect. The stronger decoupling interaction in DT820 than that in DT940 may be responsible for the better thermal magnetic stability (flux loss and β) of DT820 (See Table 1). Accordingly, the reverse change in coercivity with

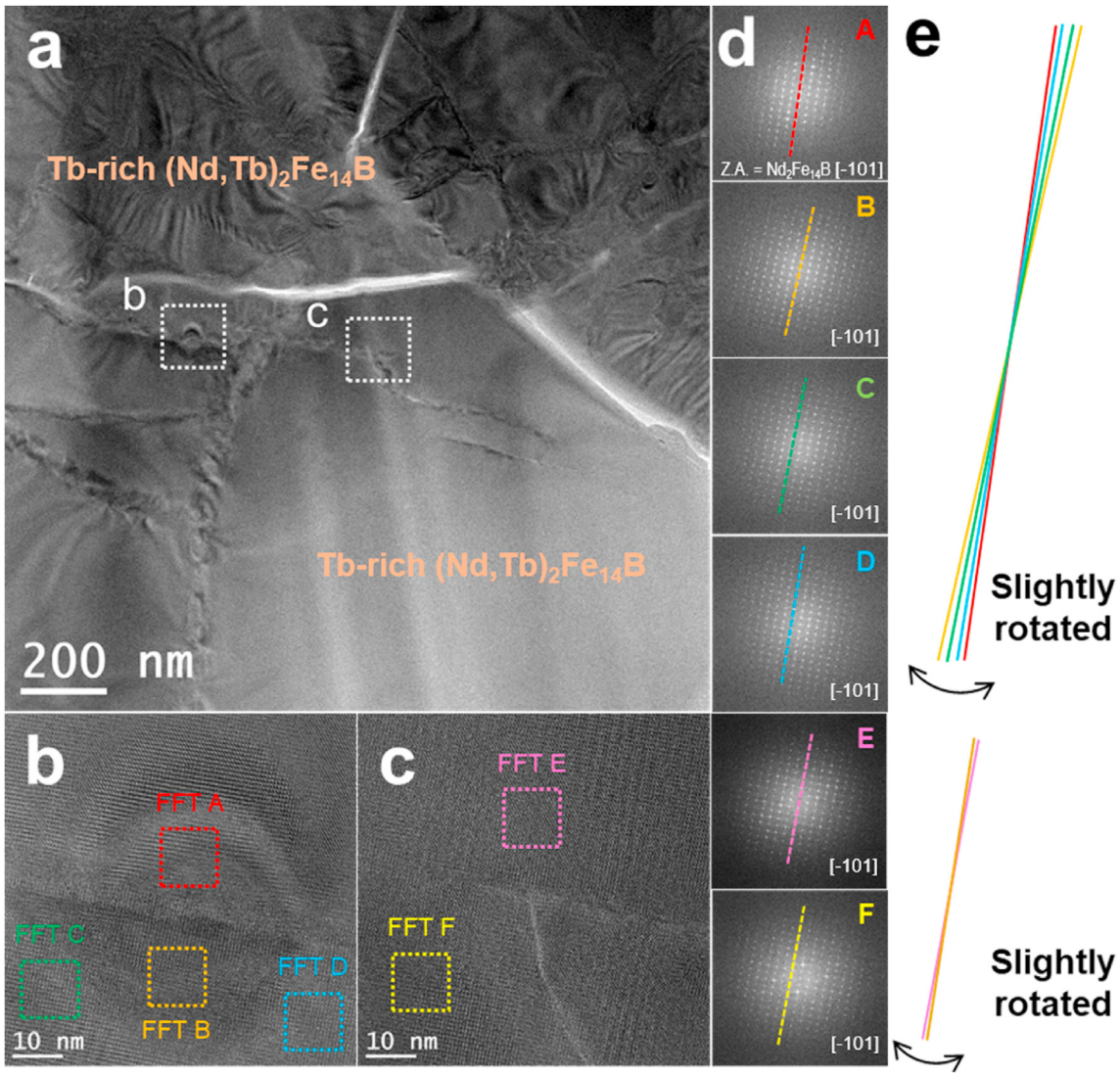

Fig. 6. (a) Bright-field TEM image of grain surface composed of Tb-rich (Nd, Tb)$_2$Fe$_{14}$B phases, (b) and (c) high-resolution TEM images obtained from the areas marked with *b* and *c* shown in (a), (d) electron diffraction patterns in the selected areas shown in (b) and (c) for the [−101] beam direction, and (e) summary of crystal orientations shown in (d).

increasing working temperature is explained, which is that a significant reduction in coercivity of DT940 at 90 °C is caused by its lower thermal stability.

We further analyzed the microstructure of the magnet with the high flux loss of −5.95% and high coercivity of 31.59 kOe, as shown in Fig. 1(b). This magnet was prepared by GBDP at 940 °C and heat treatment at 940 °C. The BSE and EPMA mapping images at depths of 80 and 300 μm below the surface are shown in Fig. 8. The Tb map reveals that the core−shell structures are not well formed because of the large amounts of thick Tb-rich shells. With the formation of these thick Tb shells, residual Nd atoms after Tb replacement produces an Nd-rich phase adjacent to the thick Tb-rich shell. This inhomogeneous microstructure weakens the exchange decoupling. In addition, large amounts of Nd-rich phase exist at the edges and corners of grains. Therefore, it can be inferred that this magnet has significant nucleation of reverse domains due to the exchanged coupling of grains, deteriorating its thermal stability. These experiments confirmed that the diffusion temperature is critical in controlling the magnetic thermal stability of the magnet by precisely tuning the magnet's microstructure.

4. Conclusions

Herein, we investigated the magnetic properties and thermal stability of Tb-diffused Nd−Fe−B magnets. The process to improve the magnetic properties at high working temperatures was carried out by simply adding two annealing processes after GBDP had taken place, and by changing the heat-treatment temperatures, without any metal or alloy additives. The GBDP and additional heat treatment improved the magnetic properties of the Tb-diffused Nd−Fe−B magnets than those of base magnet. Notably, the change in diffusion temperatures clearly changed details in the microstructure of the magnet, from the surface to the inside. This resulted in different behaviors, in terms of thermal stability, of the magnetic properties. As a result, a lower diffusion temperature produced more well-formed core−shell structures, yielding enhanced exchange decoupling, which is responsible for better thermal stability. From this investigation, it was determined that the decoupled microstructure can be controlled by adjusting the GBDP and additional heat-treatment temperatures. This study proposes a new manufacturing method for producing thermally stable magnets, which is a challenging issue in industrial fields.

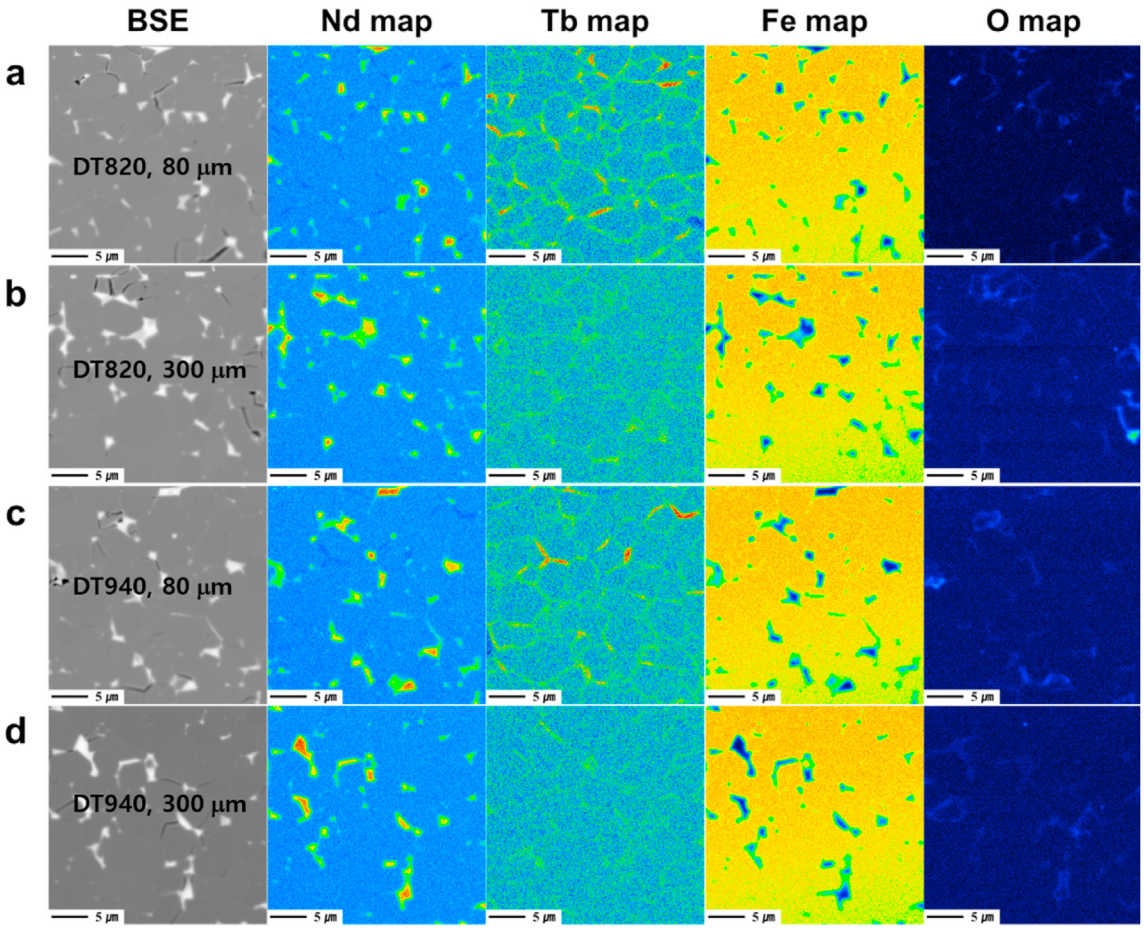

Fig. 7. Cross-sectional EPMA profiles of (a, b) DT820 and (c, d) DT940 magnets at the depths of 80 and 300 μm.

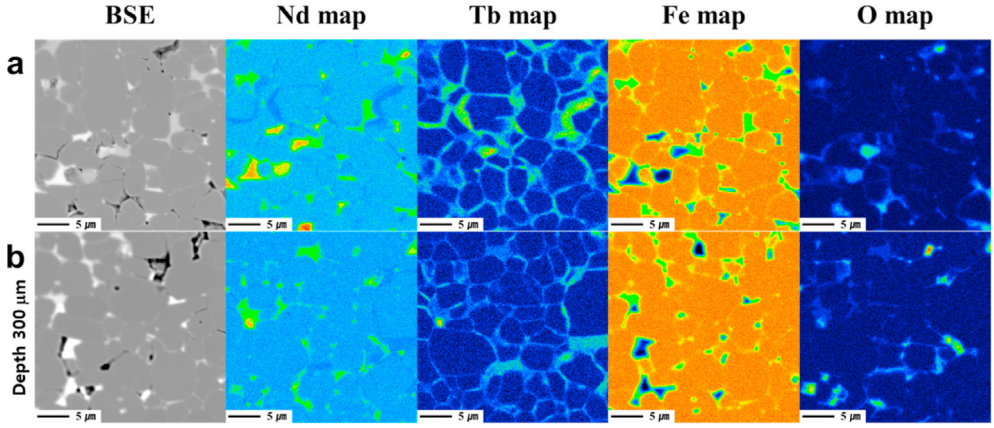

Fig. 8. Cross-sectional EPMA profiles of the magnet obtained after GBDP at 920 °C and additional heat treatment at 820 °C at the depth of 80 and 300 μm.

Credit author statement

Sumin Kim: Conceptualization, Investigation, Formal analysis, Validation, Writing- Original draft preparation. **Hyun-Sook Lee:** Conceptualization, Validation, Writing - rriginal draft preparation, Writing - Review & Editing preparation. **Woo Hyun Nam:** Investigation, Visualization. **Donghwan Kim:** Conceptualization, Validation. **Weon Ho Shin:** Investigation, Visualization. **Jong Wook Roh:** Validation, Writing - Review & Editing preparation. **Wooyoung Lee:** Supervision.

Declaration of competing interest

The authors declare that they have no known competing financial interests or personal relationships that could have appeared to influence the work reported in this paper.

Acknowledgements

This research was supported by the Priority Research Centers Program (2019R1A6A1A11055660) of the National Research Foundation of Korea (NRF). H-S Lee thanks the Basic Science Research Program of NRF (2015R1C1A2A01055702). Both are funded by the Ministry of Science and ICT in South Korea.

Appendix A. Supplementary data

Supplementary data to this article can be found online at https://doi.org/10.1016/j.jallcom.2020.157478.

References

[1] O. Gutfleisch, M.A. Willard, E. Brück, C.H. Chen, S.G. Sankar, J.P. Liu, Magnetic materials and devices for the 21st century: stronger, lighter, and more energy efficient, Adv. Mater. 23 (2011) 821–842.
[2] A. Emadi, Handbook of Automotive Power Electronics and Motor Drives, Marcel Dekker, New York, May 2005.
[3] J. Li, L. Liu, H. Sepehri-Amin, X. Tang, T. Ohkubo, N. Sakuma, T. Shoji, A. Kato, T. Schrefl, K. Hono, Coercivity and its thermal stability of NdFeB hot-deformed magnets enhanced by the eutectic grain boundary diffusion process, Acta Mater. 161 (2018) 171–181.
[4] F. Chen, Y. Jin, Y. Cheng, L. Zhang, Investigation of the wettability and the interface feature of the melted $Nd_{70}Cu_{30}$ alloy on the surface of a sintered Nd-Fe-B magnet, Scripta Mater. 157 (2018) 135–137.
[5] H. Sepehri-Amin, T. Ohkubo, K. Hono, The mechanism of coercivity enhancement by the grain boundary diffusion process of Nd–Fe–B sintered magnets, Acta Mater. 61 (2013) 1982–1990.
[6] H. Sepehri-Amin, T. Ohkubo, S. Nagashima, M. Yano, T. Shoji, A. Kato, T. Schrefl, K. Hono, High-coercivity ultrafine-grained anisotropic Nd–Fe–B magnets processed by hot deformation and the Nd–Cu grain boundary diffusion process, Acta Mater. 61 (2013) 6622–6634.
[7] B.D. Cullity, Introduction to Magnetic Materials, vol. 11, John Wiley & Sons, Inc., New Jersey, 2009. Ch.
[8] D. Derewnicka-Krawczynska, S. Ferrari, V. Bilovol, M. Pagnola, K. Morawiec, F.D. Saccone, Influence of Nb, Mo, and Ti as doping metals on structure and magnetic response in NdFeB based melt spun ribbons, J. Magn. Magn Mater. 462 (2018) 83–95.
[9] A.M. El-Aziz, A. Kirchner, O. Gutfleisch, A. Gebert, L. Schultz, Investigations of the corrosion behaviour of nanocrystalline Nd–Fe–B hot pressed magnets, J. Alloys Compd. 311 (2000) 299–304.
[10] L.Q. Yua, J. Zhang, S.Q. Hu, Z.D. Han, M. Yan, Production for high thermal stability NdFeB magnets, J. Magn. Magn Mater. 320 (2008) 1427–1430.
[11] Q. Jiang, W. Lei, Q. Zeng, Q. Quan, L. Zhang, R. Liu, X. Hu, L. He, Z. Qi, Z. Ju, M. Zhong, S. Ma, Z. Zhon, Improved magnetic properties and thermal stabilities of Pr-Nd-Fe-B sintered magnets by Hf addition, AIP Adv. 8 (2018), 056203.
[12] A.K. Pathak, M. Khan, K.A. Gschneidner Jr., R.W. McCallum, L. Zhou, K. Sun, M.J. Kramer, V.K. Pecharsky, Magnetic properties of bulk, and rapidly solidified nanostructured $(Nd_{1-x}Ce_x)_2Fe_{14-y}Co_yB$ ribbons, Acta Mater. 103 (2016) 211.
[13] R. Zhang, Y. Liu, J. Ye, W. Yang, Y. Ma, S. Gao, Effect of Nb substitution on the temperature characteristics and microstructures of rapid-quenched NdFeB alloy, J. Alloys Compd. 427 (2007) 78–81.
[14] X. Zhang, S. Guo, C. Yan, L. Cai, R. Chen, D. Lee, A. Yan, Improvement of the thermal stability of sintered Nd-Fe-B magnets by intergranular addition of $Dy_{82.3}Co_{17.7}$, J. Appl. Phys. 115 (2014) 17A757.
[15] Y. Lu, S. Zhong, M. Yang, C. Wang, L. Yang, L. Li, B. Yang, Nd-Fe-B Magnets, The gradient change of microstructures and the diffusion principle after grain boundary diffusion process, Materials 12 (2019) 3881.
[16] A. Kim, F. Camp, E. Dulis, Effect of oxygen, carbon, and nitrogen contents on the corrosion resistance of Nd-Fe-B magnets, IEEE Trans. Magn. 26 (1990) 1936–1938.
[17] Q. Zhou, Z.W. Liu, X.C. Zhong, G.Q. Zhang, Properties improvement and structural optimization of sintered NdFeB magnets by non-rare earth compound grain boundary diffusion, Mater. Des. 86 (2015) 114–120.
[18] E.A. Perigo, H. Takiishi, C.C. Motta, R.N. Faria, On the squareness factor behavior of RE-FeB (RE = Nd or Pr) magnets above room temperature, IEEE Trans. Magn. 45 (2009) 4431–4434.
[19] D.J. Branagan, M.J. Kramer, Y.L. Tang, R.W. McCallum, Maximizing loop squareness by minimizing gradients in the microstructure, J. Appl. Phys. 85 (1999) 5923–5925.
[20] M. Haavisto, S. Tuominen, T. Santa-Nokki, H. Kankaanpää, M. Paju, P. Ruuskanen, Magnetic behavior of sintered NdFeB magnets on a long-term timescale, Ann. Mater. Sci. Eng. 2014 (2014) 760584.
[21] G. Rieger, M. Seeger, H. Kronmüller, Microstructural parameters in high-remanent sintered NdFeB magnets, Phys. Status Solidi A 171 (1999) 583–595.
[22] D. Goll, M. Seeger, H. Kronmüller, Magnetic and microstructural properties of nanocrystalline exchange coupled PrFeB permanent magnets, J. Magn. Magn Mater. 185 (1998) 49–60.
[23] W. Chen, Y.L. Huang, J.M. Luo, Y.H. Hou, X.J. Ge, Y.W. Guan, Z.W. Liu, Z.C. Zhong, G.P. Wang, Microstructure and improved properties of sintered Nd-Fe-B magnets by grain boundary diffusion of non-rare earth, J. Magn. Magn Mater. 476 (2019) 134–141.
[24] K.-D. Durst, H. Kronmüller, Microstructure and improved properties of sintered Nd-Fe-B magnets by grain boundary diffusion of non-rare earth, J. Magn. Magn Mater. 68 (1987) 63–75.
[25] J. Liu, H. Sepehri-Amin, T. Ohkubo, K. Hioki, A. Hattori, T. Schrefld, K. Hono, Grain size dependence of coercivity of hot-deformed Nd–Fe–B anisotropic magnets, Acta Mater. 82 (2015) 336–343.